Journal of Asian Earth Sciences xxx (2012) xxx–xxx

Contents lists available at SciVerse ScienceDirect

Journal of Asian Earth Sciences

journal homepage: www.elsevier.com/locate/jseaes

Analysis of landslide dams induced by the 2008 Wenchuan earthquake

Xuanmei Fan [a,b,*], Cees J. van Westen [b], Qiang Xu [a], Tolga Gorum [b], Fuchu Dai [c]

[a] The State Key Laboratory of Geohazards Prevention and Geoenvironment Protection, Chengdu University of Technology, Chengdu, Sichuan, China
[b] Faculty of Geo-Information Science and Earth Observation (ITC), University of Twente, 7500 AE, Enschede, P.O. Box 217, The Netherlands
[c] Institute of Geology and Geophysics, Chinese Academy of Sciences, P.O. Box 9825, Beijing, China

ARTICLE INFO

Article history:
Received 15 January 2012
Received in revised form 7 April 2012
Accepted 4 June 2012
Available online xxxx

Keywords:
Landslide dam
Wenchuan earthquake
Quake lake
Failure rate

ABSTRACT

Landslide dams caused by earthquakes are extremely hazardous disruptions of the flow of water and sediment in mountain rivers, capable of delivering large outburst floods that may devastate downstream areas. We analyzed a unique inventory of 828 landslide dams triggered by the M_w 7.9 2008 Wenchuan tectonic earthquake, China, constituting ~1.4% of the >60,000 coseismic slope failures mapped and attributed to this event. While 501 landslides blocked the rivers completely, the remainder caused only partial damming or channel diversion. The spatial distribution of landslide dams follows the same trend of that of the total landslide distribution, with landslide dams being most abundant in the steep watersheds of the hanging wall of the Yingxiu-Beichuan Thrust Fault, and in the northeastern part of the strike-slip fault near Qingchuan. Besides the co-seismic landslide density, the river width also played a key role in determining the landslide dam formation. Narrow rivers are more prone to be dammed than the wide rivers. The correlation between river width and landslide dam volume follows a linear relation, which can be used to roughly estimate the dam formation possibility. However, the applicability of this correlation needs to be validated in other regions. The decay (failure) rate of dams, defined here as the percentage of the number and area of landslide dams that have failed over time, shows that ~25% of dams accounting for ~30% of total landslide dam area failed one week after the earthquake. These percentages increased to ~60% within 1 month, and to >90% within 1 year. The geomorphometric parameters were analyzed, revealing power-law relations between landslide area and dam width, landslide source area and dam area, as well as lake area and lake volume. The inventory presented in this study will enrich the worldwide earthquake-induced landslide dam database and will also contribute to a better understanding of the post-earthquake dam decay.

1. Introduction

Landslide dams are ubiquitous and often potentially dangerous results of river-blocking landslides, and occur frequently in tectonically active mountains with narrow and steep valleys (Costa and Schuster, 1988). Strong earthquakes are among the prime triggering factors of landslides and landslide dams (Keefer, 1984; Evans et al., 2011). Studies on earthquake-induced landslide inventories, and the analysis of their controlling factors, causal mechanism and susceptibility or hazard assessment have been carried out by Jibson et al. (2000), Lee et al. (2008), Owen et al. (2008), and Yin et al. (2010). The M_w 7.9 Wenchuan earthquake that struck China's Sichuan Province on 12 May 2008 triggered ~60,000 landslides (Dai et al., 2011; Gorum et al., 2011), i.e. significantly in excess of those triggered by other recent earthquakes, such as the 1999 Chi-Chi earthquake (M_w 7.6; Khazai and Sitar, 2003) and the 2005 Kashmir earthquake in Pakistan (M_w 7.6; Sato et al., 2007).

A number of landslide-dam inventories (Costa and Schuster, 1988, 1991; Chai et al., 1995; Casagli and Ermini, 1999; Korup, 2004; Hewitt, 2006, 2011; Hermanns et al., 2011; Weidinger, 2011) have been created by compiling and reconstructing historic large events. However, there is hardly any work specifically on earthquake-induced landslide dams (Adams, 1981; Hancox et al., 1997; Evans et al., 2011), due to the scarcity of well-documented inventories. Much previous work is scattered in local case studies (e.g. Dunning et al., 2006; Harp and Crone, 2006; Nash et al., 2008; Duman, 2009; Schneider, 2009) and mainly focused on the historic occurrences, instead of a systematic compilation of a comprehensive dataset on size and stability. Little work exists on systematical analysis of the regional distribution patterns and the related controlling factors, the post-event failure rate and the longevity of coseismic landslide dams. In this paper we aim to contribute to the systematic analysis of earthquake-induced landslide dams. We present one of the first and largest complete event-based landslide-dam inventories, with detailed geomorphometric

* Corresponding author at: Faculty of Geo-Information Science and Earth Observation (ITC), University of Twente, 7500 AE, Enschede, P.O. Box 217, The Netherlands. Tel.: +31 (0)53 487 4416.
E-mail address: fan21676@itc.nl (X. Fan).

1367-9120/$ - see front matter © 2012 Elsevier Ltd. All rights reserved.
http://dx.doi.org/10.1016/j.jseaes.2012.06.002

parameters of landslide dams and quake lakes. Using detailed remote sensing interpretation and fieldwork, we created a unique database of >800 landslide dams triggered by the Wenchuan earthquake. In order to reduce the potential for dam-break floods, the Chinese army created artificial spillways in 32 of the dams using explosives and heavy machinery. Q. Xu et al. (2009) qualified the hazard of these 32 dams by considering dam height, dam composition and maximum capacity of the landslide-dammed lakes.

To our best knowledge, this event-based inventory is unprecedented in size, and provides a unique opportunity to study the immediate post-earthquake dynamics of landslide dams, their geomorphometric features and the spatial distribution pattern at the regional scale. We assess methods to quantify the mean failure time of landslide dams and failure rate. A detailed understanding of the post-earthquake behavior of landslide dams will contribute to a better understanding of landslide dam formation and longevity.

2. Tectonic and geomorphic setting

The devastating 2008 (M_w 7.9) Wenchuan earthquake with a focal depth of 14–19 km occurred on the NE-trending Longmenshan thrust fault zone (LTFZ) that separates the Sichuan basin from the steep and heavily dissected eastern margin of the Tibetan Plateau in China. The LTFZ consists of three major sub-parallel faults: the Wenchuan-Maowen (WMF), Yingxiu-Beichuan (YBF) and Pengguan faults (PF) (Fig. 1). The coseismic rupture initiated near Yingxiu town (31.061°N, 103.333°E) and propagated unilaterally towards the northeast, generating a 240-km long surface rupture along the Yingxiu Beichuan fault, and a 72-km long rupture along the Pengguan fault (X. Xu et al., 2009; Lin et al., 2009; Shen et al., 2009). Prior to the occurrence of the Wenchuan earthquake, Li et al. (2008) reported 66 earthquakes with M_s > 4.7 mainly concentrated on the Minjiang fault and the southern part of the Longmenshan fault zone since 638 AD. For instance, in 1933, the Diexi earthquake (M_s 7.5) was induced by the tectonic activity along the Minjiang fault zone.

The LTFZ runs through a mountain range with elevations ranging from 500 m in the Sichuan Basin to >5,000 m over a distance of ~50 km, with tributaries of the Yangtze River flowing oblique or perpendicular from the north or northwest to south or southeast. Major river basins draining the study area include the Min and its tributaries, the Hei Shui and Tsakahao rivers in the west, as well as the Jian, Fu and Baishui rivers in the east. Besides, a series of small channels (*P*1–*P*7) drain the Pengguan Massif in front of the Longmenshan zone adjacent to the Sichuan Basin (Fig. 1). The lower part of the Min river (also called Minjiang) turns southwest and flows along the Wenchuan-Maowen fault, and then crosses the

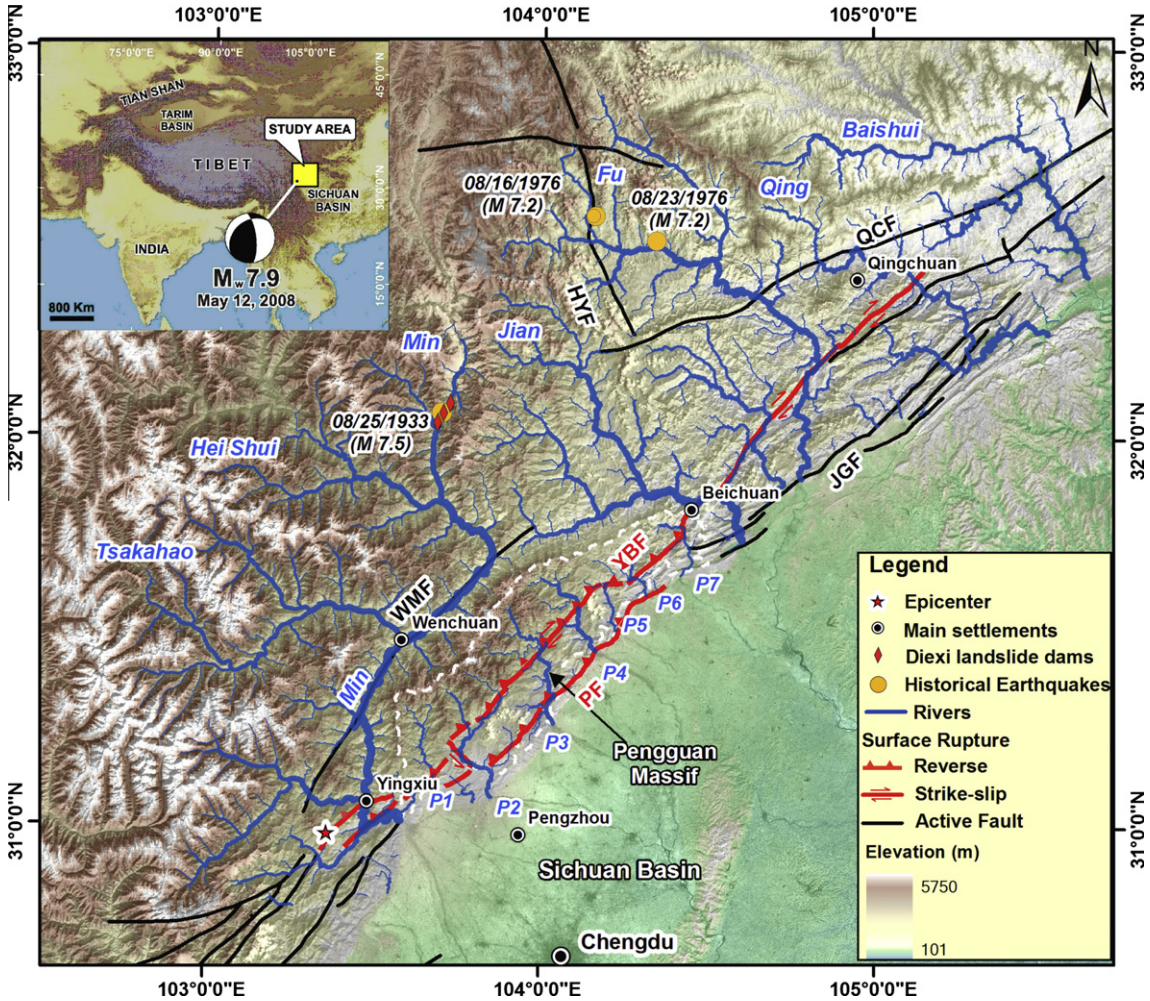

Fig. 1. Topography of the study area (inset shows location). Major rivers are shown in blue. The major catchments are: Min river (*MJR*), Jian river (*JJR*), Fu river (*FJR*), Qing River (*QR*), and 7 smaller rivers (*P*1–*P*7) in the Pengguan Massif bounded by the white dashed line. WMF: Wenchuan-Maowen fault; YBF: Yingxiu-Beichuan fault; PF: Pengguan fault; JGF: Jiangyou-Guanxian fault; QCF: Qingchuan fault; HYF: Huya fault; MJF: Minjiang fault (after X. Xu et al., 2009). The epicenter location is from USGS, 2008. (For interpretation of the references to colour in this figure legend, the reader is referred to the web version of this article.)

Please cite this article in press as: Fan, X., et al. Analysis of landslide dams induced by the 2008 Wenchuan earthquake. Journal of Asian Earth Sciences (2012), http://dx.doi.org/10.1016/j.jseaes.2012.06.002

Pengguan Massif to drain into the Sichuan Basin. The Hei Shui and Tsakahao rivers join the Min river west of the Pengguan Massif. Deeply incised bedrock rivers are flanked by hillslopes commonly >30° steep within the LTFZ, and underlain by deformed Paleozoic sediments and metamorphic rocks, Mesozoic sediments, and Precambrian crystalline and metamorphic rocks (Burchfiel et al., 1995; Kirby et al., 2003).

Some large-scale landslide dams and catastrophic dam break floods were reported in the study area. On June 1, 1786, a strong earthquake (M 7.75) occurred in the Kangding-Luding area, resulting in a large landslide dam that blocked the Dadu river. Ten days later, the sudden breaching of the dam caused catastrophic downstream flooding and 100,000 fatalities (Dai et al., 2005). Besides, the Diexi earthquake (M_s 7.5) of August 25, 1933 produced nine large landslide dams. Three of these dams (Dahaizi, Xiaohaizi, and Deixi, see Fig. 1) had a maximum height of 160 m above the Min River. After seven weeks the three lakes merged, and emptied in a dam-break flood that rushed downstream for a distance of 250 km, killing more than 2,500 people (Chai et al., 2000).

3. Landslide dam inventory

Event-based landslide inventories at a catchment- or regional scale aim at mapping all slope failures following a single landslide triggering episodes, such as an earthquake, intense rainstorms or significant snowmelt, and is essential for generating landslide susceptibility and hazard maps (e.g. Kamp et al., 2008; Lee et al., 2008; van Westen et al., 2008 and Cui et al., 2009). Landslide susceptibility and hazard assessments are often based on the assumption that the past is the key to the future, and therefore inventories of past landslides and their causal relationships can be used to predict future ones. For triggering earthquake events that have relatively large return periods, this creates the difficulty that it is very unlikely that such an event occurred in recent times, and that the landslides can be mapped. This is one of the reasons that earthquake induced landslide susceptibility assessment still is done using fairly simple methods (Jibson et al., 2000).

3.1. Source data for landslide and landslide dam mapping

Gorum et al. (2011) described the method for mapping landslides in the earthquake-affected Wenchuan region using 52 pre- and post-earthquake satellite images. The same data was used in this study, complemented by EO-1 (10-m spatial resolution) of July 2008 and ASTER images (15 m) of July, 2010 for mapping the landslide dams and impounded lakes. Fig. 2 indicates the spatial coverage of the satellite images. The pre-earthquake images consisted of multispectral data such as ASTER (15-m spatial resolution) and ALOS AVNIR-2 (10 m) as well as panchromatic data from ALOS PRISM (2.5 m) and the Indian Cartosat-1 (2.5 m). Post-earthquake images included SPOT-5 (2.5 m), IKONOS (2.5 m), ASTER, ALOS AVNIR-2 and PRISM data as well as a limited number of aerial photos (0.3 m) which covered some large landslides (see the Supplementary material Table S1). To precisely identify the position of the landslide dams, the aerial photographs and satellite images were geometrically corrected using ground-control points (GCPs) measured in the field by DGPS and points selected from the 1:50,000-scale digital topographical maps. A pre-earthquake DEM with 25 m × 25 m grid spacing was produced from 1:50,000 scale digital topographical maps, by interpolating the contour lines with contour intervals ranging between 10 m for low relief mountain areas and 20 m for high relief areas. According to the Chinese national standard, the horizontal and vertical accuracy of the 25 m DEM at a 90% level of confidence is better than 20 m and 10 m, respectively.

3.2. Mapping and image interpretation

Landslide dams were mapped through visual interpretation by comparing pre- and post-earthquake false color composites or panchromatic images, assisted by field checks in accessible areas containing about 60% of dams. The coseismic landslides are clearly recognizable from change detection of monoscopic images, using image characteristics such as tone, texture, pattern and shape. Although stereoscopic image interpretation would have been better for optimal landslide interpretation, it was not practically feasible to generate stereo images for such an extensive area of about 35,000 km^2. Therefore, the stereo-based interpretation was carried out for selected areas around large landslide dams. These were identified by diagnostic features such as a higher reflectance compared to the surrounding areas with vegetation cover; and geomorphic features such as scarps; bare rock-fall talus; and asymmetric hummocky deposits featuring flow lobes, and transverse or longitudinal ridges. The resolution of the available images did not allow

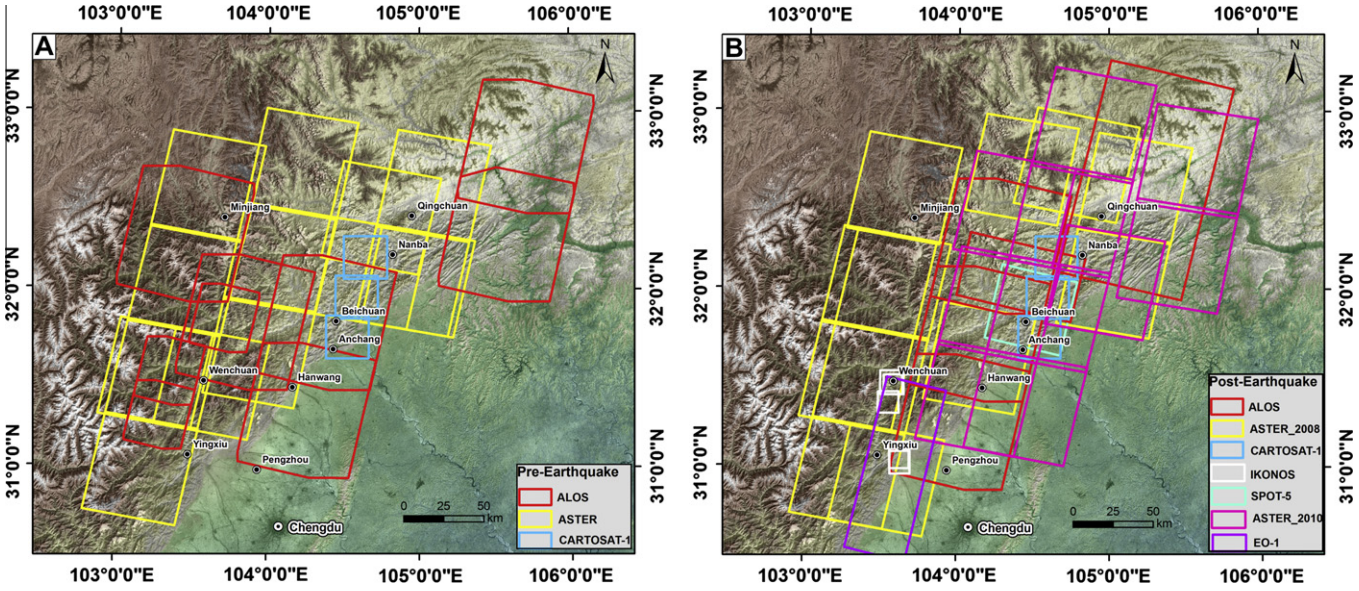

Fig. 2. Pre- and post-earthquake image coverage map. See also Table S1.

to map landslides and lakes that were less than 200 m^2. We classified landslide dams into two classes: (1) full blockage, where landslide debris completely obstructed rivers, forming a lake and (2) partial blockage, where debris obstructed the river without forming an impoundment.

We mapped scar and deposit areas for landslides completely or partly blocking the rivers, as well as any associated quake lakes. The area of quake lakes changes with time because of incoming water and sediment discharge. Therefore, we compared the multi-temporal images and assumed the largest area derived from images to represent the full lake area, and mapped the lakes before any artificial breaching was carried out. Some medium-resolution images precluded the distinction between landslide scar and deposit areas (Fig. 3a and b). While the high-resolution images allow us to map in detail the initiation, transportation and accumulation area for 64% of the landslide dams. Cross checking of pre- and post-earthquake images revealed that some pre-existing landslides were enlarged or reactivated during the earthquake, while several dams failed shortly after they were formed (Fig. 3c–f). We used pan sharpening of high-resolution panchromatic images (PRISM) to increase the resolution of multispectral images (ALOS AVNIR-2) to allow for more details, such as coarse grained rock slide deposits and the linear bedding structure (Fig. 3 g and h).

Fig. 4 shows the distribution of the landslide dams in relation to the overall landslide distribution mapped by Gorum et al. (2011). Fig. 5 shows the detailed inventory of landslide dams in a small part of the area indicated in Fig. 4. The types of river-blocking landslides, following the terminology of Cruden and Varnes (1996) are indicated in the inset of Fig. 4. Rock slides are the most common type and account for 35% of the data, because the fractured rock slopes were found very susceptible to seismic shaking (Chigira et al., 2010). The largest coseismic landslide caused by the Wenchuan earthquake (indicated in Fig. 4) was the Daguangbao landslide, with an area of 7.1 km^2 and an estimated volume of 7.5×10^8 m^3 (Huang et al., 2012). The Tangjiashan landslide dam had impounded the largest lake with an estimated maximum volume of 3×10^8 m^3. The dam is located ~85 km upstream of Mianyang city, i.e. the second largest in Sichuan with a population of ~1.2 million. The Chinese authorities decided to evacuate parts of Mianyang city (Liu et al., 2009), until the Tangjiashan landslide dam was artificially breached, and the lake was drained.

Our inventory contains 828 river-blocking landslides; 501 (61%) caused complete damming of rivers, while 327 (39%) only partially dammed the rivers. Partially damming landslides ranged in area from 768 m^2 to 1.3×10^6 m^2, which are slightly smaller than the completely damming landslides with areas ranging from 1,249 m^2 to 7.1×10^6 m^2. Quake lake areas varied from 217 m^2 to 6.5×10^6 m^2. The landslides triggered by the Wenchuan earthquake cover an estimated total area of ~811 km^2 (Dai et al., 2011), and the damming landslides covered an area of ~54 km^2, which is ~7% of the total landslide area.

4. Spatial distribution analysis of landslide dams

We estimated the spatial density of all coseismic landslides (Gorum et al., 2011) and landslide dams within a circular moving window of 1 km^2 radius, obtaining maximum values of 54.1 landslides/km^2 and 4.5 landslide dams/km^2 respectively (Fig. 6A and B).

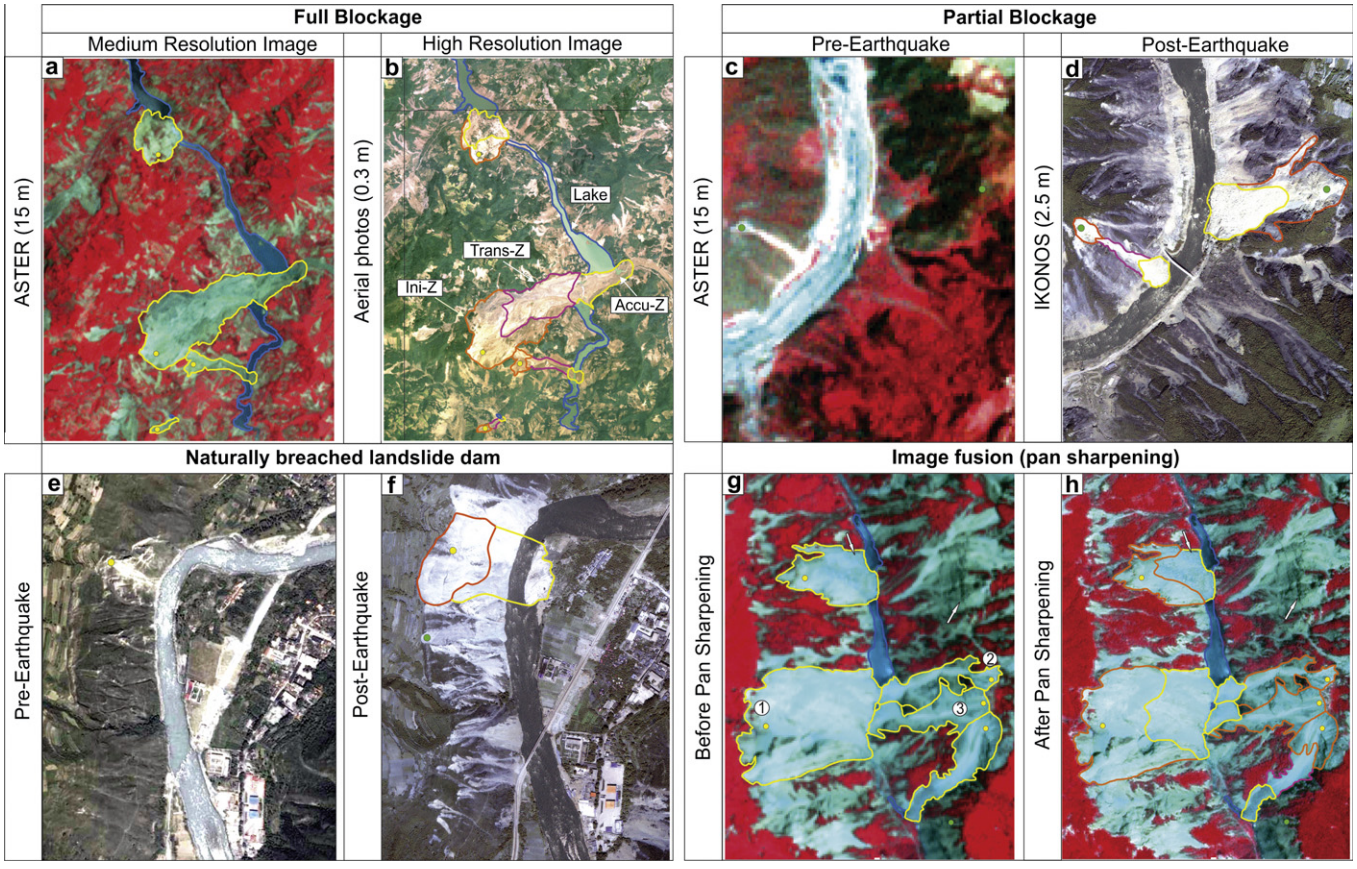

Fig. 3. Examples of medium (a and c) and high resolution images (b and d) showing landslide dam polygon mapping. Detailed mapping allowed delineating the initiation (Ini-Z), transportation (Trans-Z) and accumulation (Accu-Z) parts of damming landslides, whereas the landslides can only be mapped as single polygons using medium resolution images. Complete and partial blockages as well as the reactivated landslides can be observed by comparing pre- and post-earthquake images. Some landslide dams were dissected by rivers already several hours after they were formed (e and f). A landslide dam can be formed by several landslides (e.g. ◦1, ◦2and ◦ 3) jointly as shown in g.

Please cite this article in press as: Fan, X., et al. Analysis of landslide dams induced by the 2008 Wenchuan earthquake. Journal of Asian Earth Sciences (2012), http://dx.doi.org/10.1016/j.jseaes.2012.06.002

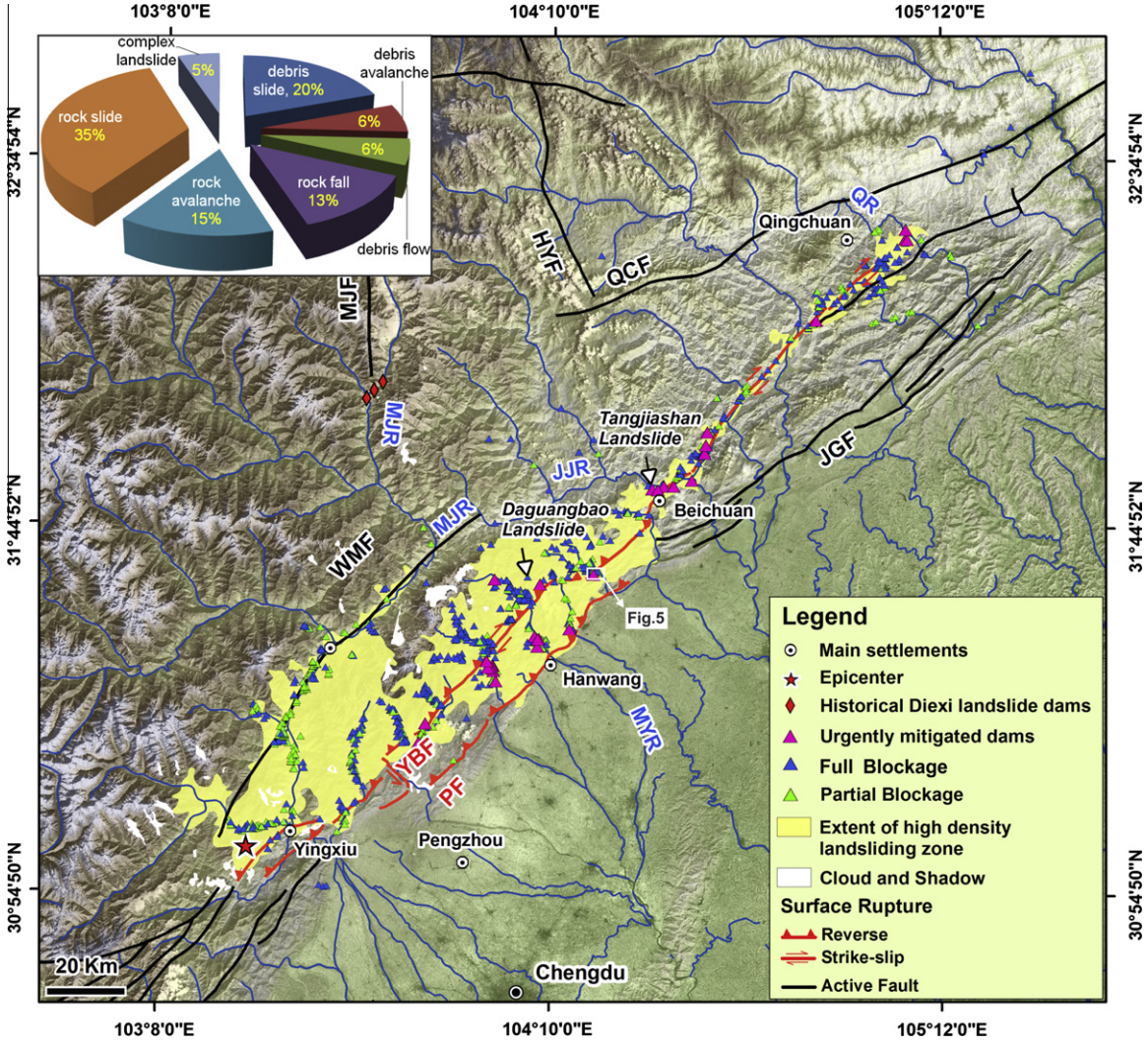

Fig. 4. Distribution of landslide dams triggered by the Wenchuan earthquake, China. The high landslide density zone is defined by a landslide area density >0.1 km^{-2}; also shown are epicenters of historical earthquakes (USGS, 2008) and historical Diexi landslide dams. White polygons are unmapped due to the presence of clouds and shadows in post-earthquake imagery. The major fault and river names are indicated in Fig. 1.

A swath profile along the fault in a 240 km long and 25 km wide rectangular zone (Fig. 6C) as well as four perpendicular 25 km by 20 km long swaths (Fig. 6C1–C4) illustrate the mean normalized point density of landslides and landslide dams. A swath profile width of 25 km was selected, because it represents the extent of the surface projection of the hanging wall of the Yingxiu-Beichuan fault. Fig. 6C shows the variation of mean normalized point densities for landslides and landslide dams along the fault from SW to NE. Both follow the same trend, with peaks in the SW section from Yingxiu to Beichuan and near the fault tip near Qingchuan. The landslide-dam density peaks at several river junctions. Landslide density in sections of the fault with dominant thrust component was much higher than on sections with steep fault dip angles dominated by strike slip. Four swath cross sections (Fig. 6C1–C4) show that peaks in landslide density near the drainage network coincide with a high density of landslide dams. Both landslide and landslide-dam densities are higher on the hanging wall of the Yingxi-Beichuan fault (YBF) than on the footwall. However, this difference is not so apparent for the cross-section 2, where the footwall of YBF is also the hanging wall of the Penguan fault (PF).

Landslide dams are most abundant in a region with 7 steep watersheds (named *P*1–*P*7, since they don't have specific names) in the Pengguan Massif and the Min river (*MJR*) (Fig. 6B). Different from the dams in the Pengguan Massif, most of dams (>90%) along the deeply incised Min River have mainly caused the partial blockage, since the Min river has large discharge and width. In general, landslide density directly affects landslide-dam density, although we found that the correlation between landslide volume and river width also played a key role. We estimated the landslide volume by applying volume-area (*V*-*A*) scaling parameters using the equation presented by Larsen et al. (2010), because it was obtained from >4000 landslides and also took landslide material (soil or bedrock) into account.

$$V = 0.146A^{1.332} \quad (1)$$

The river width was estimated by the following scaling relation (Finnegan et al., 2005; Whittaker et al., 2007):

$$W \sim A^{3/8}S^{-3/16} \quad (2)$$

where W is the channel width; A is drainage area (as a proxy for discharge, Q); and S is channel bed slope, which was extracted from the DEM following the method of Kirby et al. (2003). We analyzed the landslide dam volume variation in the main catchments, and the results are presented in Fig. 7, in which also the channel width of rivers is indicated (the red line in Fig. 7). Landslide dams that blocked the wider rivers (e.g. Jian and Fu rivers) usually have larger

Please cite this article in press as: Fan, X., et al. Analysis of landslide dams induced by the 2008 Wenchuan earthquake. Journal of Asian Earth Sciences (2012), http://dx.doi.org/10.1016/j.jseaes.2012.06.002

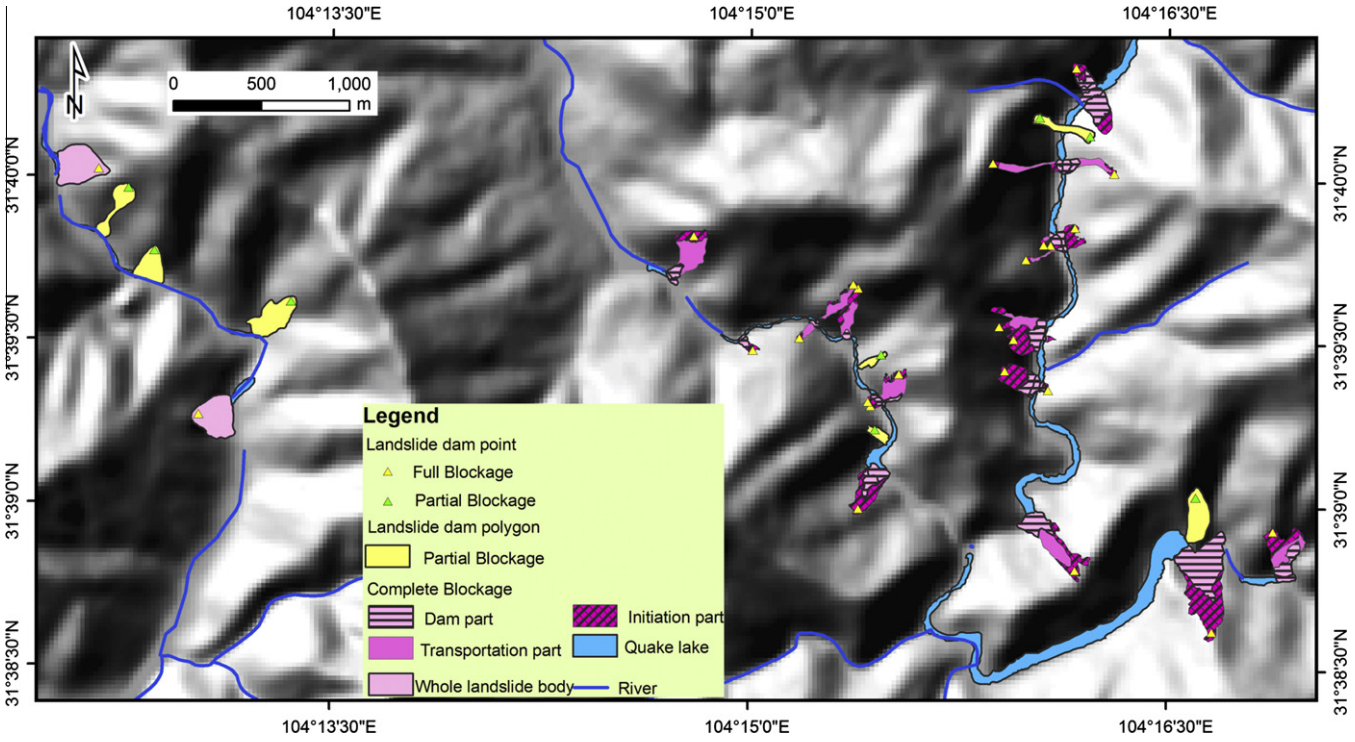

Fig. 5. An example showing landslide dam polygon mapping in an area indicated in Fig. 4.

volumes. An exception is for the Min river, where partial blocking landslides were more abundant (Figs. 7 and 8). Narrow rivers with a small catchment area are more prone to be dammed, thus landslide dam density is higher along the *P*1–*P*7 rivers (with a width of <15 m and catchment area of 132–463 km^2) than along the Jian and Fu rivers with a width of >30 m and catchment area of 4100 km^2 and 2400 km^2, respectively (Fig. 7). The correlation between river width and landslide dam volume follows a linear relation (Fig. 8)

5. Analysis of geomorphometric parameters

A number of geomorphometric parameters of the landslide dams and associated quake lakes have been considered important for a first-order empirical assessment of dam stability and potential hazard of dam-break floods (Fig. 9). We derived these attributes following the terminologies defined in previous work (Costa and Schuster, 1988; Dong et al., 2009).

Most of the parameters such as the landslide dam length, width, area and quake lake area, can be directly extracted from landslide dam and lake polygons, while others (e.g. landslide dam height and volume as well as the quake lake depth and volume) require further calculations. We assumed the height difference between the highest and the lowest point under the related lake polygon as the lake depth, which was calculated based on the pre-earthquake DEM with the vertical accuracy of 10 m. The dam height was considered to be equal to the lake depth if the lake is full. The lake volume was calculated using GIS-based volumetric algorithms (the "TIN Polygon Volume" function). To reduce possible errors that might be caused by the DEM accuracy, we only calculated the volume for 319 lakes with a depth more than 10 m and an area exceeding 1000 m^2. The results were validated using field measurement data of 24 lakes that were surveyed by a Chinese expert team and the Chinese army directly after the earthquake (Q. Xu et al., 2009; Fig. 10). The lake volume was estimated by field measured lake area and average lake depth by using the handheld GPS, Laser distance finder, and boat with sonar (or rope and weight) (Zhang, 2010).

The calculated and field measured lake volumes with logarithmic axes are shown in the inset of Fig. 10, which show a good fit. To better underpin the contribution of smaller lakes, we excluded the Tangjiashan lake from Fig. 10. The results demonstrate that our lake volume calculations show a good match with the field measurement data (R^2 = 0.89). For the Tangjiashan dam, the calculated dam height and lake volume is 115 m and ~3.5×10^8 m^3, respectively, which are close to the field measurements with the dam height ranging from 82 to 124 m and the lake volume of 3.0×10^8 m^3. The calculated volumes of large lakes are more variable than those of smaller lakes, since slight changes in lake depth will lead to large volumetric changes.

Based on our inventory, we extracted the geomorphometric parameters from the full blockages indicated in Fig. 9 and analyzed some empirical relationships between these parameters as shown in Fig. 11. The results show a power-law relationship (R^2 = 0.72) between the landslide area and the resulting landslide dam width along the valley, implying that the landslide area is a good indicator for predicting dam width (Fig. 11A). A total length of ~76 km of river reaches was directly covered by damming landslide debris. Fig. 11B shows that the landslide source (initiation) area can be used to estimate the landslide dam area. The relation between the quake lake volume and the dam height is less clear (R^2 = 0.53), and can be related to several additional factors such as the local valley morphometry, upper catchment area and terrain (Fig. 11C). The empirical scaling relationship between lake area and volume that we constrained by field measurements is clear, showing a positive power-law relation (R^2 = 0.8), with the V_L varying over 6 magnitude orders from 10^3 m^3 to 10^9 m^3 (Fig. 11D). The lake volume is an essential parameter for dam failure hazard and risk assessment, which has been used in various empirical equations to predict dam-break flood peak discharge (Evans, 1986; Costa and Schuster, 1988; Walder and O'Connor, 1997). Therefore, the relation in Fig. 11D can also be applied in similar regions for a rapid

Please cite this article in press as: Fan, X., et al. Analysis of landslide dams induced by the 2008 Wenchuan earthquake. Journal of Asian Earth Sciences (2012), http://dx.doi.org/10.1016/j.jseaes.2012.06.002

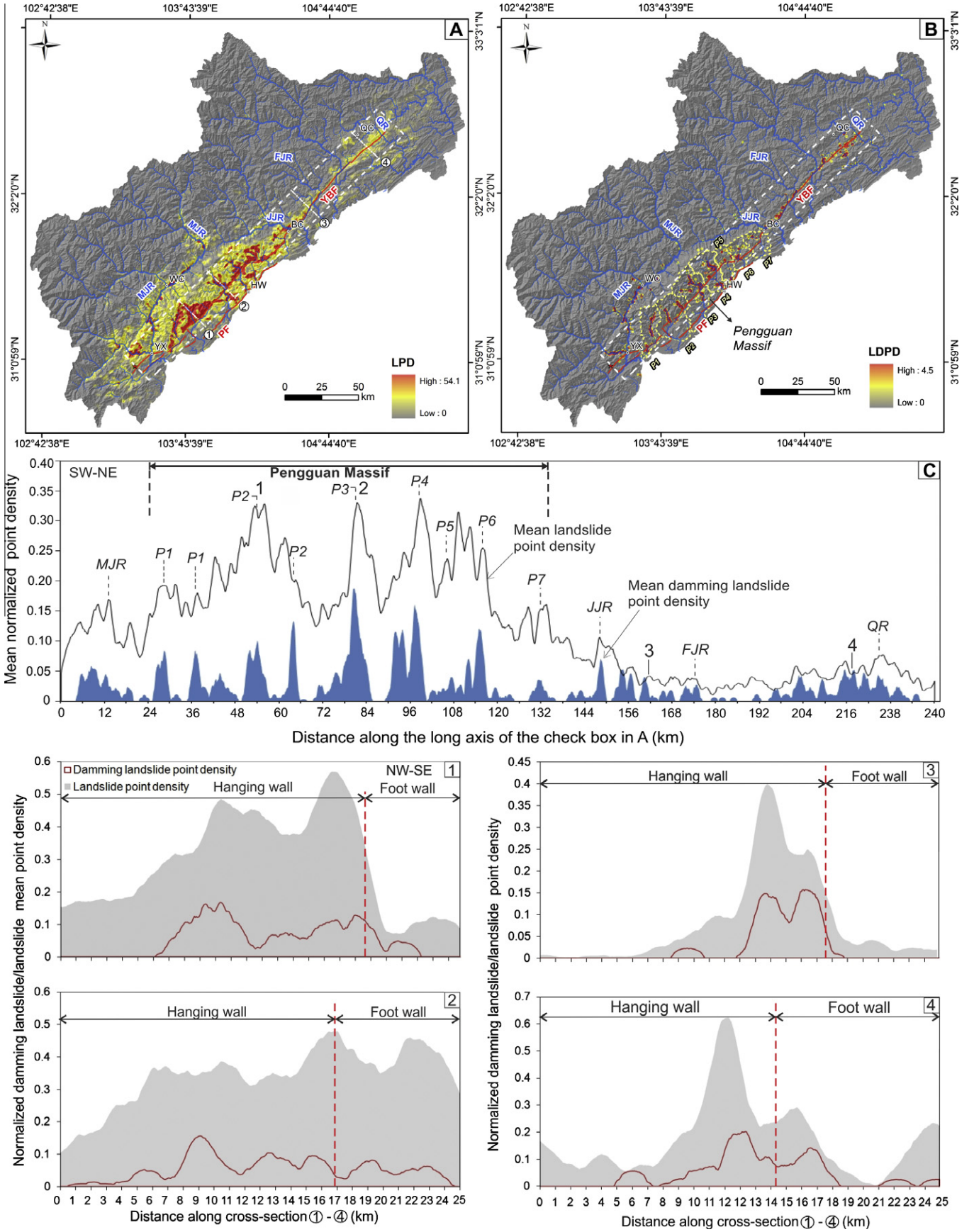

Fig. 6. Comparison of densities of blocking and non-blocking landslides. A. and B. show the landslide and landslide dam point density, respectively. White dashed lines are 240-km by 25-km swath profiles and cross sections (1–4). LPD and LDPD represent the landslide and landslide dam point density, respectively. C. Mean normalized landslide and landslide dam densities along the SW-NE profile and four NW-SE cross sections, respectively. Red lines in are Yingxiu-Beichuan fault (YBF) and Pengguan fault (PF). Yellow dash lines are the boundary of the P1–P7 watersheds in the Pengguan Massif. YX, WC, BC, and QC are the cities of Yingxiu, Wenchuan, Beichuan and Qingchuan, respectively. MJR, JJR, FJR, and QR represent Min, Jian, Fuj and Qing rivers, respectively. (For interpretation of the references to colour in this figure legend, the reader is referred to the web version of this article.)

Please cite this article in press as: Fan, X., et al. Analysis of landslide dams induced by the 2008 Wenchuan earthquake. Journal of Asian Earth Sciences (2012), http://dx.doi.org/10.1016/j.jseaes.2012.06.002

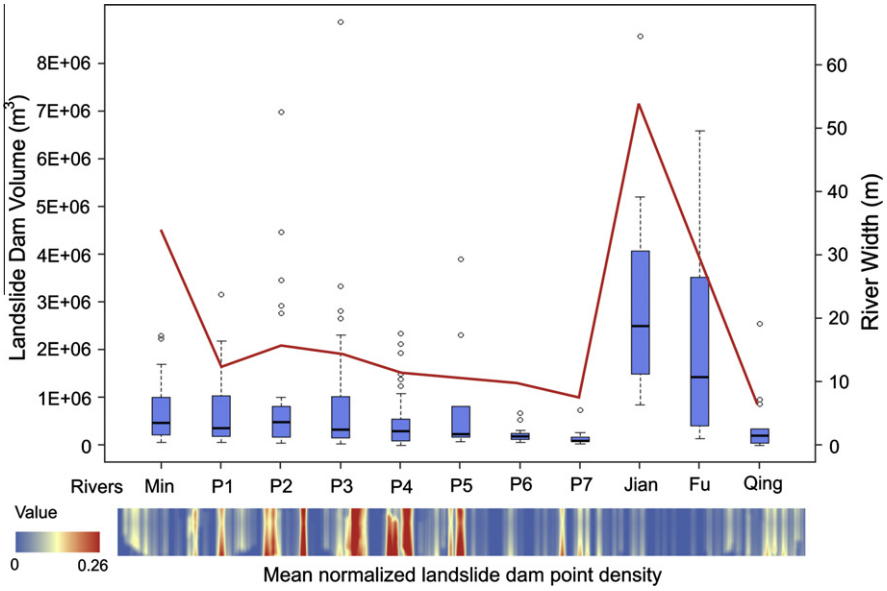

Fig. 7. Box and whisker plot of landslide dam volume in major catchments with comparison of river width. The spectrum shows the variation of mean landslide dam point density along the SW-NE swath profile in Fig. 6.

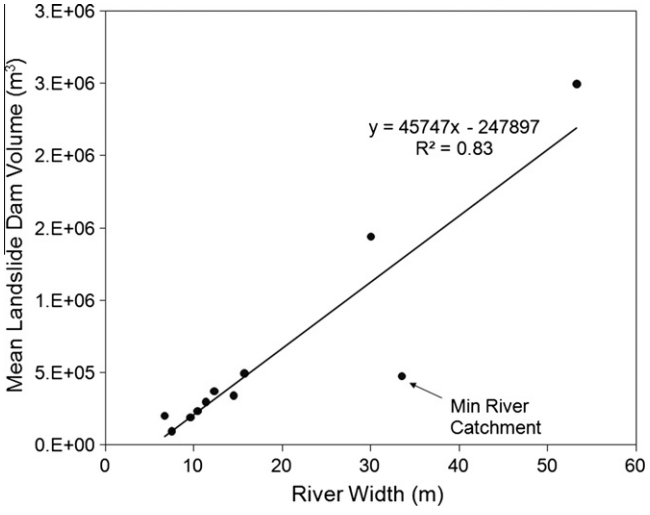

Fig. 8. Correlation between the mean landslide dam volume in different catchments (in Fig. 7) and the river width. Because most dams are partial blockage with comparatively small volume regarding to the river width, the Min river catchment appears to be an outlier.

estimation of lake volume, and the related hazard evaluation and mitigation.

6. Analysis of the failure rate of landslide dams

Most landslide dams, particularly those that caused only partial obstruction, were dissected shortly after the earthquake. We define the failure rate of full-blockage dams as the percentage of the dams that have failed over the time intervals bracketed by multi-temporal remote sensing data (Table 1; Fig. 12). The percentage can be expressed based on landslide area or on the number of landslides. An analysis of landslide dams that had remained intact as revealed from ASTER images dated July 2010 and covering nearly the full study area, indicates that 23 of the 501 (4.6%) completely river-blocking landslide dams were still in place 26 months after the earthquake. These 23 landslide dams accounted for 20% of the total landslide dam area, and were mainly formed by complex deep-seated slope failures. Computation of the failure rate in the intermediate periods was limited to imagery covering the Beichuan and Pengzhou regions (Table 1; Table S1). Altogether, some 60% of dams, constituting ~43% of the total landslide dam area, failed within 1 month after the earthquake, showing a sharp decrease from 501 to 215 intact dams (Table 1; Fig. 12). This decrease leveled off 2 months after the earthquake. Three heavy rainstorms hit the earthquake region in the first 3 years after the earthquake. One event occurred 4 months after the earthquake, on September 24, 2008, triggering 72 debris flows in the epicenter region (Tang et al., 2009). In the Beichuan area, 56 debris flows and reactivated landslides were detected through cross-checking remote sensing images. Three of them blocked rivers, while the others delivered a large amount of sediments to the rivers. Many of the coseismic landslide dams failed during or after this rainfall event. Another rainfall event occurred in 2009, but its effects are poorly documented. A rainstorm on 12–14 August, 2010 triggered 11 debris flows in Qingping, Mianzhu and about 50 debris flows in Dujiangyan, forming new dams. One of the dams in Dujiangyan caused the inundation of the relocation site for the new town of Yingxiu. Based on this information, three triangle symbols were plotted in Fig. 12 to show the three post-earthquake rainfall events.

7. Discussion and conclusions

The temporary or permanent blockage of streams by landslides is a characteristic secondary hazard in mountainous areas affected by strong earthquakes or major rainfall events. It is also possible to happen without recognized triggers, i.e. the Mayunmarca landslide dam occurred in 1974, Peru (Hutchinson and Kojan, 1975). Such impoundments may pose a large risk to downstream areas given the potential for catastrophic lake outbreak flooding. Our inventory of landslide dams caused by the Wenchuan earthquake is unprecedented in that it records abundant river blockage following a single regional landslide triggering event. It presents the spatial distribution pattern of landslide dams with comparison to all coseismic landslides. They are most abundant in the Pengguan massif, along the thrusting part of the Yingxiu-Beichuan fault (YBF), due to following reasons:

Please cite this article in press as: Fan, X., et al. Analysis of landslide dams induced by the 2008 Wenchuan earthquake. Journal of Asian Earth Sciences (2012), http://dx.doi.org/10.1016/j.jseaes.2012.06.002

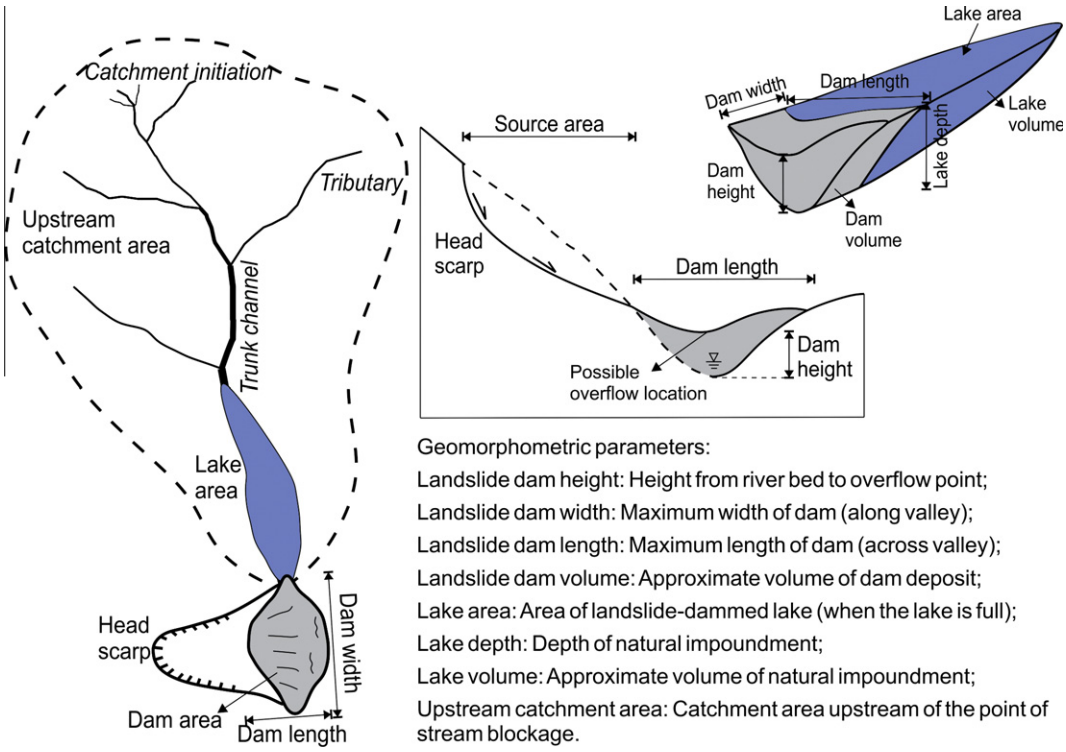

Fig. 9. Sketch of geomorphometric properties of landslide dam and impounded lakes.

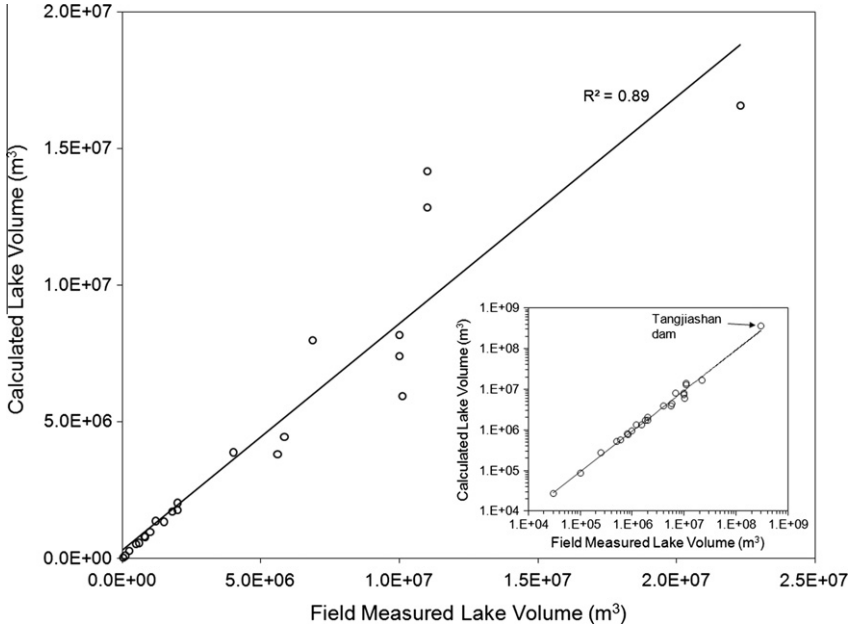

Fig. 10. Validation of the quake-lake volume estimates using field measurement data. Inset has logarithmic axes for better displaying the extreme dimensions of the Tangjiashan dam.

(1) Steep and rough terrain with hillslope inclinations >30° are prone to generate landslides. Fig. 13 depicts the elevation variation along the Yingxiu-Beichuan fault, showing that the mean elevation in the Pengguan Massif is about 400 m higher than that in the northeast from Beichuan to the end of the fault. This difference contributes to the higher landslide and landslide dam densities in the Pengguan massif.

(2) The Pengguan Massif is composed of fragmented Precambrian crystalline gneisses and granitoids separated from a series of Triassic mudstones by the Yingxiu-Beichuan fault (Chigira et al., 2010). Field investigation revealed that the pervasively fragmented rocks favor landslide (dam) occurrences. Most of large rock avalanches occurred there in intensely jointed granite rock masses.

Please cite this article in press as: Fan, X., et al. Analysis of landslide dams induced by the 2008 Wenchuan earthquake. Journal of Asian Earth Sciences (2012), http://dx.doi.org/10.1016/j.jseaes.2012.06.002

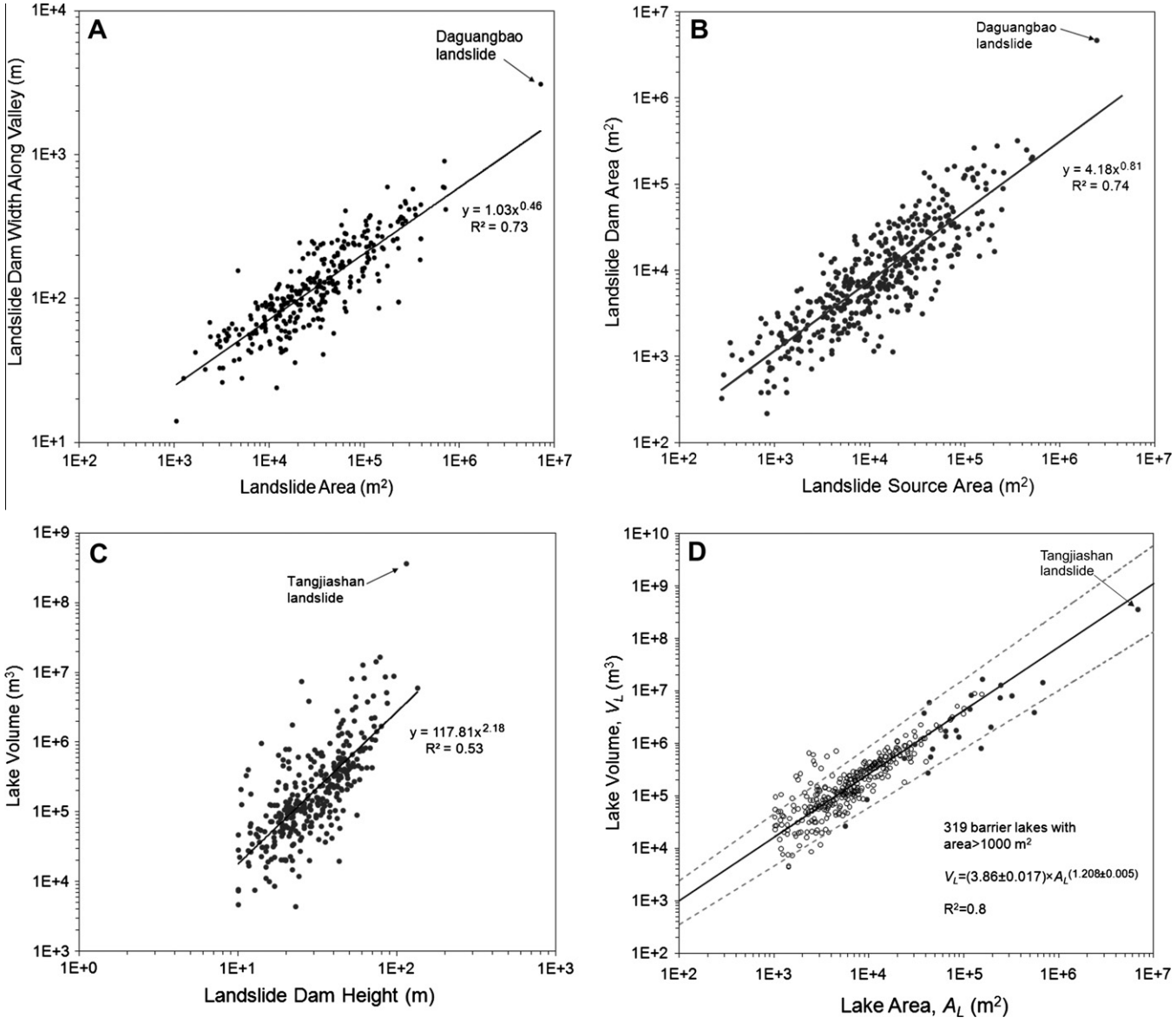

Fig. 11. (A) Plot of landslide dam width along valley (W_D) versus landslide dam area (A_D); (B) Plot of landslide source area (A_s) versus landslide dam area (A_D); (C) Plot of quake lake volume (V_L) versus landslide dam height (H_D); (D) Plot of quake lake volume (V_L) versus lake area (A_L). Filled circles in D. represent lakes with flied measured volume as shown in Fig. 10. Thick black lines are best fit obtained by the Reduced Major Axis Regression (RMA). Dashed grey lines show 95% confidence intervals.

Table 1
Summary of multi-temporal remote sensing data used for assessing the full-blockage landslide dam failure rate.

Data covered region	Date	Sensor	Resolution (m)	Number of failed dams	Failure rate	
					Percentage of dam number (%)	Percentage of dam area (%)
Around Beichuan area, including 65 landslide dams	May 18, 2008	ALOS PRISM/Aerial photos	2.5/0.3	16	24.60	29.80
	October 13, 2008	SPOT-5	2.5	61	93.80	78.60
	January 24, 2009	CARTOSAT-1	2.5	62	95.40	79.80
	July 19, 2010	ASTER	15	62	95.40	79.80
Pengzhou area, including 77 landslide dams	June 4, 2008	ALOS AVNIR-2	10	44	57.10	42.30
	July 8, 2008	EO-1	10	59	76.60	57.20

(3) The changes of fault geometry and slip rate from the southwest to the northeast were quantified by GPS and InSAR data (Yarai et al., 2008; Hao et al., 2009), showing that in the Pengguan Massif the fault plane dips moderately to the northwest, becoming nearly vertical in the northeast (from Beichuan to Qingchuan region), associated with a change

Please cite this article in press as: Fan, X., et al. Analysis of landslide dams induced by the 2008 Wenchuan earthquake. Journal of Asian Earth Sciences (2012), http://dx.doi.org/10.1016/j.jseaes.2012.06.002

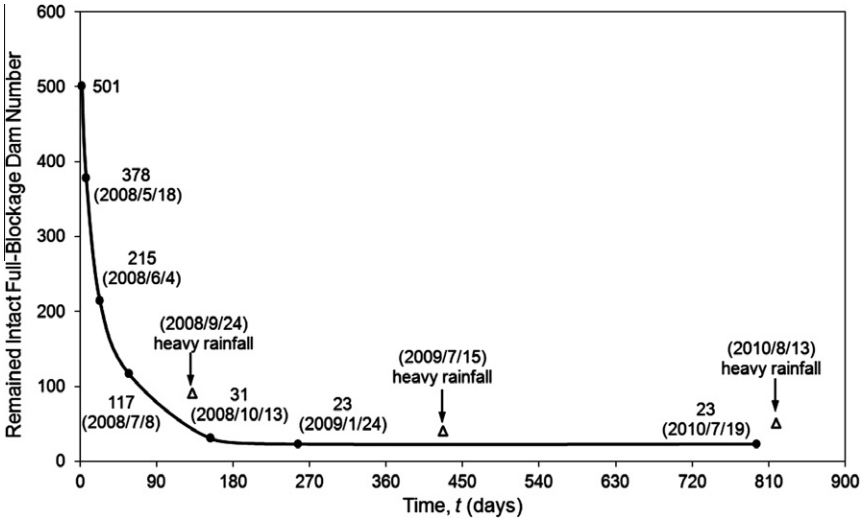

Fig. 12. Decay of the number of remaining intact full-blockage landslide dams with time.

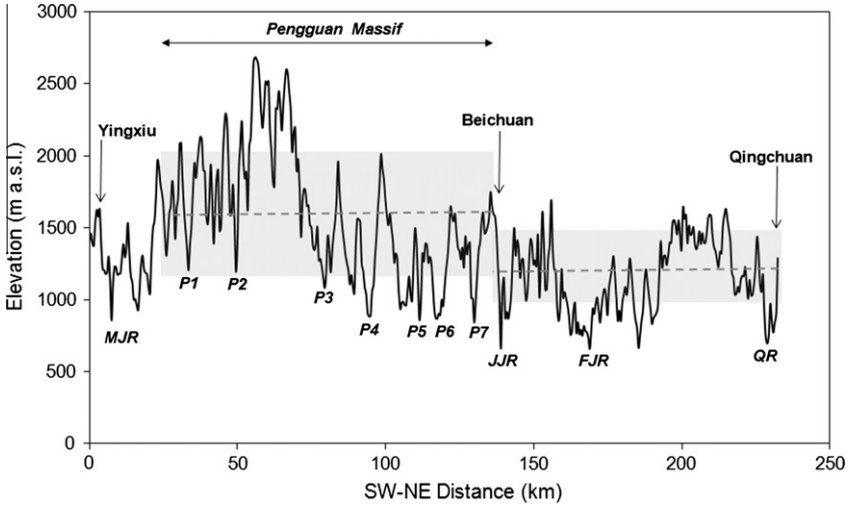

Fig. 13. Elevation profile along the Yingxiu-Beichuan fault. The dashed lines represent the mean elevation in the Pengguan Massif and the northeast part of the fault. Grey boxes delimit the ±1 standard deviation (SD) from the mean.

from predominantly thrusting to strike-slip motion. High fault-slip rate (large seismic energy) concentrated in the thrusting part of the fault in the Penguan Massif (Gorum et al., 2011).

(4) Deeply incised narrow valleys (*P*1–*P*7 in Fig. 13) with small catchment areas varying from 132 to 463 km^2 were readily blocked.

The correlation between landslide dam volume and river width relies on the empirical scaling relationships we used, although the changes of the scaling relationship will not change the relative comparison of landslide dam volume and river width in different catchments. The landslide volume-area scaling relationship we used from Larsen et al. (2010) takes the landslide type and material into account, thus was considered appropriate. The one for estimating the river width (Eq. 2) is also considered to be most suitable for the rivers in the tectonically active mountainous regions compared to the conventional scaling relationship ($W \sim A^{0.5}$) (Finnegan et al., 2005). The correlation between river width and landslide dam volume we extracted from this study follows a linear relation, demonstrating that damming of wide rivers generally requires landslides with large volume. However, the applicability of this correlation is still unknown before being validated in other regions.

To put our analysis of dam longevity and decay into a broader context, we compiled three databases as shown in Fig. 14. The data from Costa and Schuster (1988), and Ermini and Casagli (2003) comprise 73 and 205 worldwide historical cases, respectively. Fig. 14 shows that the Wenchuan earthquake database fits to the function:

$$P_f = 0.973e^{-10.88/t} (R^2 = 0.97) \quad (3)$$

It demonstrates the relationship between cumulative percent of failed landslide dams (P_f) with time in days (t). Fig. 14 indicates that about 30% of dams that reportedly failed did so within one week after their formation, while >90% failed within a year. This figure also suggests that the survival time of landslide dams induced by

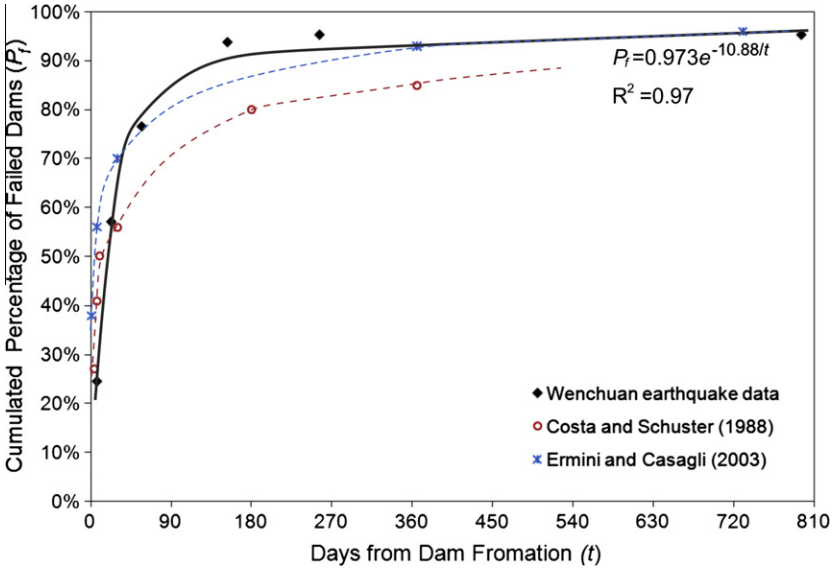

Fig. 14. Longevity of full-blockage dams with comparison of two worldwide datasets.

the Wenchuan earthquake is generally shorter than that of the other two databases, most probably because the Wenchuan database contains a larger amount of small landslide dams than the other two. Besides, the landslide dam survival time is controlled by, among others, the geomorphometric parameters, dam composition materials, the lake capacity and the discharge of the inflowing stream (Weidinger, 2011).

The Wenchuan earthquake provided a unique opportunity to generate an event-based landslide dam inventory of 828 individual landslide dams, of which 501 completely blocked rivers. This very rare occasion provides insights on the spatio-temporal clustering and decay of coseismic landslide dams. We focused on the immediate post-earthquake dynamics of landslide dams at the regional scale and longevity of the landslide dams in a global context, because they are extremely important for hazard assessment and mitigation. Further research is directed towards analyzing the seismic, geological, topographic and hydrological factors that determine the occurrence of landslide dams, with the ultimate aim to come to a conceptual model for landslide dam susceptibility and hazard assessment. Besides, the long-term effect of landslide dams on valley morphology and sediment budgets is another aspect that deserves further research attention. The deposition of lacustrine, alluvial, or deltaic sediments in reservoirs can result in changes of stream gradient, surface morphology, and superficial geology upstream from the dam, whereas dam-break floods or debris flow may rework downstream reaches.

Acknowledgements

This research was financially supported by the National Natural Science Foundation of the People's Republic of China (41130745) and the Creative Team Program of Ministry of Education of China (IRT0812), in collaboration with the United Nations University – ITC Centre for Spatial Analysis and Disaster Risk Management of the University of Twente, the Netherlands. We acknowledge Prof. Oliver Korup for his valuable comments and editing of the manuscript. Comments by Prof. Alexander Strom, Prof. Theo van Asch and other anonymous reviewers are very helpful on improving earlier drafts. We appreciate that the Japan Aerospace Exploration Agency (JAXA), GeoEye foundation, and Indian Space Research Organisation (ISRO) for providing the data for this research.

Appendix A. Supplementary material

Supplementary data associated with this article can be found, in the online version, at http://dx.doi.org/10.1016/j.jseaes.2012.06.002.

References

Adams, J., 1981. Earthquake-dammed lakes in New Zealand. Geological Society of America, Geology 9, 215–219.
Burchfiel, B., Zhiliang, C., Yuping, L., Royden, L., 1995. Tectonic of the Longmen Shan and adjacent regions, central China. International Geology Review 37, 661–735.
Casagli, N., Ermini, L., 1999. Geomorphic analysis of landslide dams in the Northern Apennine. Transactions of the Japanese Geomorphological Union 20, 219–249.
Chai, H., Liu, H., Zhang, Z., 1995. The catalog of Chinese landslide dam events. Journal of Geological Hazards and Environment Preservation 6 (4), 1–9 (In Chinese).
Chai, H., Liu, H., Zhang, Z., Xu, Z., 2000. The distribution, causes and effects of damming landslides in China. Journal of the Chengdu Institute of Technology 27, 302–307.
Chigira, M., Xu, X., Inokuchi, T., Wang, G., 2010. Landslides induced by the 2008 Wenchuan earthquake, Sichuan, China. Geomorphology 118 (3–4), 225–238.
Costa, J.E., Schuster, R.L., 1988. The formation and failure of natural dams. Geological Society of America Bulletin 100, 1054–1068.
Costa, J.E., Schuster, R.L., 1991. Documented historical landslide dams from around the world. US Geological Survey Open-File Report 91-239, p. 486.
Cruden, D.M., Varnes, D.J., 1996. Landslide types and processes. In: Turner, A.K., Schuster, R.L. (Eds.), Landslides, Investigation and Mitigation. Special Report, vol. 247. Transportation Research Board, National Research Council, pp. 36–75.
Cui, P., Zhu, Y., Han, Y., Chen, X., Zhuang, J., 2009. The 12 May Wenchuan earthquake-induced landslide lakes: distribution and preliminary risk evaluation. Landslides 6, 209–223.
Dai, F., Lee, C., Deng, J., Tham, L.G., 2005. The 1786 earthquake-triggered landslide dam and subsequent dam-break flood on the Dadu River, southwestern China. Geomorphology 65, 205–221.
Dai, F., Xu, C., Yao, X., Xu, L., Tu, X., Gong, Q., 2011. Spatial distribution of landslides triggered by the 2008 Ms 8.0 Wenchuan earthquake, China. Journal of Asian Earth Sciences 40 (4), 883–895.
Dong, J.J., Tung, Y.H., Chen, C.C., Liao, J.J., Pan, Y.W., 2009. Discriminant analysis of the geomorphic characteristics and stability of landslide dams. Geomorphology 110, 162–171.
Duman, T.Y., 2009. The largest landslide dam in Turkey: Tortum landslide. Engineering Geology 104, 66–79.
Dunning, S.A., Rosser, N.J., Petley, D.N., Massey, C.R., 2006. Formation and failure of the Tsatichhu landslide dam, Bhutan. Landslides 3, 107–113.
Ermini, L., Casagli, N., 2003. Prediction of the behavior of landslide dams using a geomorphological dimensionless index. Earth Surface Processes and Landforms 28, 31–47.
Evans, S.G., 1986. The maximum discharge of outburst floods caused by the breaching of man-made and natural dams. Canadian Geotechnical Journal 23, 385–387.

Evans, S.G., Delaney, K.B., Hermanns, R.L., Strom, A., Scarascia-Mugnozza, G., 2011. The formation and behaviour of natural and artificial rockslide dams; implications for engineering performance and hazard management. In: Evans, S.G., Hermanns, R.L., Strom, A.L., Scarascia Mugnozza, G. (Eds.), Natural and artificial rockslide dams. Lecture Series in Earth Sciences. Springer, Berlin, pp. 1–76.

Finnegan, N.j., Roe, G., Montgomery, D.R., Hallet, B., 2005. Controls on the channel width of rivers: implications for modeling fluvial incision of bedrock. Geology 33 (3), 229–232.

Gorum, T., Fan, X., van Westen, C.J., Huang, R., Xu, Q., Tang, C., Wang, G., 2011. Distribution pattern of earthquake-induced landslides triggered by the 12 May 2008 Wenchuan earthquake. Geomorphology 133, 152–167.

Hancox, G.T., Perrin, N.D., Dellow, G.D., 1997. Earthquake-induced landsliding in New Zealand and implications for MM intensity and seismic hazard assessment. Lower Hutt: Institute of Geological and Nuclear Sciences Client Report 43601B Prepared for Earthquake Commission Research Foundation, 85 pp.

Hao, K., Si, H., Fujiwara, H., Ozawa, T., 2009. Coseismic surface-ruptures and crustal deformations of the 2008 Wenchuan earthquake Mw 7.9, China. Geophysical Research Letters 36 (11), 2–6.

Harp, E.L., Crone, A.J., 2006. Landslides Triggered by the October 8, 2005, Pakistan Earthquake and Associated Landslide-Dammed Reservoirs. US Geological Survey Open-file Report: 2006-1052, p. 13.

Hermanns, R.L., Folguera, A., Penna, I., Fauqué, L., Niedermann, S., 2011. Landslide dams in the central Andes of Argentina (Northern Patagonia and the Argentine Northwest). In: Evans, S.G., Hermanns, R.L., Strom, A.L., Scarascia Mugnozza, G. (Eds.), Natural and Artificial Rockslide Dams. Lecture Series in Earth Sciences. Springer, Berlin, pp. 147–176.

Hewitt, K., 2006. Disturbance regime landscapes: mountain drainage systems interrupted by large rockslides. Progress in Physical Geography 30, 365–393.

Hewitt, K., Gosse, J., Clague, J.J., 2011. Rock avalanches and the pace of late quaternary development of river valleys in the Karakoram Himalaya. Geological Society of America Bulletin 123, 1836–1850.

Huang, R., Pei, X., Fan, X., Zhang, W., Li, S., Li, B., 2012. The characteristics and failure mechanism of the largest landslide triggered by the Wenchuan earthquake, May 12, 2008, China. Landslides 9, 131–142.

Hutchinson, J.N., Kojan, E., 1975. The Mayunmarca Landslide of 25th April, 1974, Peru. UNESCO Report Serial No. 3124 Paris, UNESCO.

Jibson, R.W., Harp, E.L., Michael, J.A., 2000. A method for producing digital probabilistic seismic landslide hazard maps. Engineering Geology 58, 271–289.

Kamp, U., Growley, B.J., Khattak, G.A., Owen, L.A., 2008. GIS-based landslide susceptibility mapping for the 2005 Kashmir earthquake region. Geomorphology 101, 631–642.

Keefer, D.K., 1984. Landslides caused by earthquakes. Geological Society of America Bulletin 95, 406–421.

Khazai, B., Sitar, N., 2003. Evaluation of factors controlling earthquake-induced landslides caused by Chi-Chi earthquake and comparison with the Northridge and Loma Prieta events. Engineering Geology 71, 79–95.

Kirby, E., Whipple, K.X., Tang, W., Chen, Z., 2003. Distribution of active rock uplift along the eastern margin of Tibetan Plateau: inferences from bedrock channel longitudinal profiles. Journal of Geophysical Research 108, 1–24.

Korup, O., 2004. Geomorphometric characteristics of New Zealand landslide dams. Engineering Geology 73, 13–35.

Larsen, I.J., Montgomery, D.R., Korup, O., 2010. Landslide erosion controlled by hillslope material. Nature Geoscience 3, 247–251.

Lee, C.T., Huang, C.C., Lee, J.F., Pan, K.L., Lin, M.L., Dong, J.J., 2008. Statistical approach to earthquake-induced landslide susceptibility. Engineering Geology 100 (1–2), 43–58.

Li, X., Zhou, Z., Yu, H., Wen, R., Huang, M., Zhou, Y., Cu, J., 2008. Strong motion observations and recordings from the great Wenchuan earthquake. Earthquake Engineering and Engineering Vibration 7 (3), 235–246.

Lin, A., Ren, Z., Jia, D., Wu, X., 2009. Co-seismic thrusting rupture and slip distribution produced by the 2008 Mw 7.9 Wenchuan earthquake, China. Tectonophysics 471, 203–215.

Liu, N., Zhang, J., Lin, W., Cheng, W., Chen, Z., 2009. Draining Tangjiashan Barrier Lake after Wenchuan earthquake and the flood propagation after the dam break. Science in China Series E-technological Sciences 52 (4), 801–809.

Nash, T., Bell, D., Davies, T., Nathan, S., 2008. Analysis of the formation and failure of Ram Creek landslide dam, South Island, New Zealand. New Zealand Journal of Geology & Geophysics 51, 187–193.

Owen, L.A., Kamp, U., Khattak, G.A., Harp, E.L., Keefer, D.K., Bauer, M.A., 2008. Landslides triggered by the 8 October 2005 Kashmir earthquake. Geomorphology 94 (1–2), 1–9.

Sato, H.P., Hasegawa, H., Fujiwara, S., Tobita, M., Koarai, M., Une, H., Iwahashi, J., 2007. Interpretation of landslide distribution triggered by the 2005 Northern Pakistan earthquake using SPOT 5 imagery. Landslides 4, 113–122.

Schneider, J.F., 2009. Seismically reactivated Hattian slide in Kashmir, Northern Pakistan. Journal of Seismology 13 (3), 387–398.

Shen, Z., Sun, J., Zhang, P., Wan, Y., Wang, M., Bürgmann, R., Zeng, Y., Gan, W., Liao, H., Wang, Q., 2009. Slip maxima at fault junctions and rupturing of barriers during the 2008 Wenchuan earthquake. Nature Geoscience 2, 718–724.

Tang, C., Zhu, J., Li, W., Liang, J., 2009. Rainfall-triggered debris flow following the Wenchuan earthquake. Bulletin of Engineering Geology and the Environment, 68, 187–194.

USGS (US Geological Survey), 2008. Magnitude 7.9-Eastern Sichuan, China, 2008 May 12 06:28:01UTC. <http://earthquake.usgs.gov/earthquakes/eqinthenews/2008/us2008ryan/>.

van Westen, C.J., Castellanos, E., Kuriakose, S.L., 2008. Spatial data for landslide susceptibility, hazard, and vulnerability assessment: an overview. Engineering Geology 102, 112–131.

Walder, J.S., O'Connor, J.E., 1997. Methods for predicting peak discharge of floods caused by failure of natural and constructed earthen dams. Water Resources Research 33, 2337–2348.

Weidinger, J.T., 2011. Stability and life span of landslide dams in the Himalayas (India, Nepal) and the Qin Ling Mountains (China). In: Evans, S.G., Hermanns, R.L., Strom, A.L., Scarascia Mugnozza, G. (Eds.), Natural and Artificial Rockslide Dams. Lecture Series in Earth Sciences. Springer, Berlin, pp. 243–278.

Whittaker, A.C., Cowie, P.A., Attal, M., Tucker, G.E., Roberts, G.P., 2007. Bedrock channel adjustment to tectonic forcing: implications for predicting river incision rates. Geology 35 (2), 103–106.

Xu, Q., Fan, X., Huang, R., van Westen, C.J., 2009a. Landslide dams triggered by the Wenchuan earthquake, Sichuan Province, south west China. Bulletin of Engineering Geology and the Environment, 68 (3), 373–386.

Xu, X., Wen, X., Yu, G., Chen, G., Klinger, Y., Hubbard, J., Shaw, J., 2009b. Coseismic reverse- and oblique-slip surface faulting generated by the 2008 M_w 7.9 Wenchuan earthquake, China. Geology 37, 515–518.

Yarai, H., Nishimura, T., Tobita, M., Amagai, T., Suzuki, A., Suito, H., Ozawa, S., Imakiire, T., Masaharu, H., 2008. A fault model of the 2008 Wenchuan earthquake estimated from SAR measurements. 7th ASC Meeting, X2–040.

Yin, J., Chen, J., Xu, X., Wang, X., Zheng, Y., 2010. The characteristics of the landslides triggered by the Wenchuan M_s 8.0 earthquake from Anxian to Beichuan. Journal of Asian Earth Sciences 37, 452–459.

Zhang, X.J., 2010. Preliminary study on hydrological emergency monitoring scheme for dammed lakes. Automation in Water Recourses and Hydrology 1 (1), 1–5 (in Chinese).

Please cite this article in press as: Fan, X., et al. Analysis of landslide dams induced by the 2008 Wenchuan earthquake. Journal of Asian Earth Sciences (2012), http://dx.doi.org/10.1016/j.jseaes.2012.06.002